Imaging of Electron Potential Landscapes on Au(111)

L. Bürgi,[1,*] H. Brune,[1] and K. Kern[1,2]

[1]*Institut de Physique des Nanostructures, Ecole Polytechnique Fédérale de Lausanne, CH-1015 Lausanne, Switzerland*
[2]*Max-Planck-Institut für Festkörperforschung, Heisenbergstrasse 1, D-70569 Stuttgart, Germany*

The Hohenberg-Kohn theorem states that the ground state electron density completely determines the external potential acting on an electron system. Inspired by this fundamental theorem, we developed a novel approach to map directly the electron potential in surface systems: linear response theory applied to the total electron density as measured with scanning tunneling microscopy determines the external potential. Potential imaging is demonstrated for the s-p derived surface state on Au(111), where the "herringbone" reconstruction induces a periodic potential modulation, the details of which are revealed by our technique.

Density functional theory (DFT) has been extensively used to determine the electronic structure of solids and is today also becoming a very important basis for theoretical studies of molecular systems. At the heart of DFT is the Hohenberg-Kohn theorem [1], which states that *the external (one-electron) potential $U(\mathbf{x})$ is determined, within a trivial additive constant, by the ground state electron density $n(\mathbf{x})$.* Hence, if one had access to $n(\mathbf{x})$, the Hamiltonian, and thus all properties of the particular electronic system, would in principle be known.

In this paper we use scanning tunneling microscopy (STM) to measure the two-dimensional (2D) total density $n(\mathbf{x})$ of surface-state electrons. There exists no exact recipe linking the total electron density with the potential, and consequently approximations have been developed, such as the Thomas-Fermi approximation or the Lindhard theory [2]. Here we use linear response theory to derive the external potential $U(\mathbf{x})$ from the measured $n(\mathbf{x})$. We apply our method to s-p surface-state electrons on the $(22 \times \sqrt{3})$ reconstructed Au(111) surface [3]. Noble-metal surface-state electrons behave as nearly free 2D electron gas with parabolic dispersion [4]. On Au(111) we find a band edge energy $E_{\overline{\Gamma}} = (-510 \pm 10)$ meV and an effective mass of $m^* = (0.27 \pm 0.01)\, m_e$, in agreement with Refs. [5,6]. It was shown that the reconstruction induces a periodic potential acting on the surface-state electrons [5,7]. Until now, this potential was modeled as a square well potential, and its full shape has not been unraveled. This system is ideal for our potential mapping since the potential modulations are weak, and thus linear response theory works well.

The experiments were performed with a homebuilt low-temperature STM [8]. The Au(111) surface was cleaned by sputter-anneal cycles. All the measurements were taken at $T = 5.9$ K, with a tungsten tip and the bias voltage V applied to the sample. The topography of the Au(111) surface in Fig. 1(a) clearly reveals the uniaxial $(22 \times \sqrt{3})$ reconstruction with its herringbone pattern for isotropic stress release on a mesoscopic scale. The profile

in Fig. 1(c) taken along the white line reveals that the narrower hcp-stacking areas appear 0.05 Å higher than the wider fcc regions. The ridges are formed by atoms on bridge sites and appear 0.18 Å higher than the fcc regions. The differential conductance map in Fig. 1(b) was taken along the profile and under conditions where it directly reflects the surface local density of states (LDOS) $\rho_s(E, x)$ [8–10]. This map, where bright gray levels correspond to large LDOS, shows the influence of the reconstruction on the electronic structure of the surface. The onset of the s-p derived surface state around $E_{\overline{\Gamma}} = -510$ meV can clearly be seen. The striking features of the surface LDOS are the broad maxima centered at -380 meV
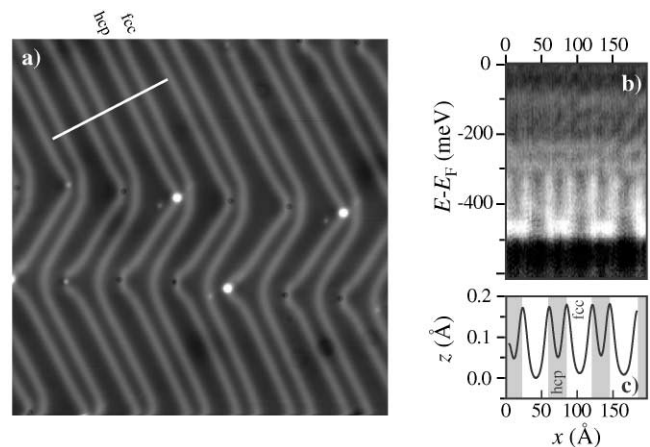

FIG. 1. (a) Constant-current image of the reconstructed Au(111) surface ($512\text{ Å} \times 512\text{ Å}$, $V = -0.42$ V, $I = 0.87$ nA). When the surface stayed at 5.9 K for several days, unknown adsorbates appeared at the elbows showing up as white spots. (b) The dI/dV map acquired by measuring 128 individual dI/dV spectra along the white line to which the profile is shown in (c) (dI/dV recorded at open feedback loop, bias modulation 20 mV peak to peak at 1.4 kHz). The tip used to perform the dI/dV map had a structured DOS leading to the location independent horizontal stripes in (b) (see, e.g., bright stripes at -0.10, -0.22, and -0.30 eV).

and situated close to the ridges of the reconstruction and the enhancements around -470 meV in the hcp regions.

The total (energy integrated) density of the surface-state electron gas $n(\mathbf{x})$ is conventionally obtained by integrating the LDOS derived from scanning tunneling spectroscopy (STS) from $E_{\overline{\Gamma}}$ to E_F. Since we are interested in 2D maps of $n(\mathbf{x})$, this seemed too time consuming, and we used the following approach yielding $n(\mathbf{x})$ more directly. We used lock-in technique with a *rectangular* bias modulation between the lower band edge $E_{\overline{\Gamma}} = eV_{\overline{\Gamma}}$ and an upper bound $E_f = eV_f$ localized between $E_{\overline{\Gamma}}$ and E_F [Fig. 2(a)]. The modulation frequency was chosen far above the bandwidth of the feedback loop; thus the tip was stabilized through the time-averaged value of the tunnel current $\bar{I} = \frac{1}{2}[I(V_{\overline{\Gamma}}) + I(V_f)]$, which is proportional to the mean value of the two integrals of the surface LDOS from $eV_{\overline{\Gamma}}$ and eV_f, respectively, to the Fermi level [11]. By inspecting Fig. 1(b) one concludes that the LDOS features due to the reconstruction have very little weight in such integrals, and thus $\bar{I}$ is only weakly influenced by changes in the electronic structure stemming from the reconstruction. Therefore the tip-sample separation is almost unaffected by those electronic structure effects and can be assumed to be constant for our purposes [8,10].

For a rectangular bias modulation the lock-in output Σ is proportional to the difference between the high and the low bias values of the current, $\Sigma(\mathbf{x}) \propto I(V_f, \mathbf{x}) - I(V_{\overline{\Gamma}}, \mathbf{x})$. Under the conditions of our experiment ($T = 5.9$ K and -510 mV $< V < 0$), and assuming a constant tip DOS, the tunneling current is a good measure for the integral of the LDOS [11]; therefore
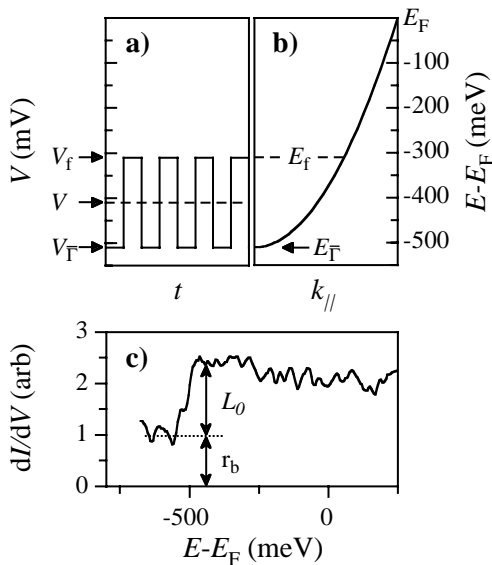

FIG. 2. (a) The bias signal used for potential mapping switches between $(V_{\overline{\Gamma}})$ and (V_f). (b) Sketch of the dispersion relation of the Au(111) s-p surface state. (c) The spectrum taken right before having performed the measurement shown in Fig. 3 yields a ratio ρ_b/L_0 of 0.7 (20 mV modulation).

$$\Sigma(\mathbf{x}) \propto \int_{eV_{\overline{\Gamma}}}^{eV_f} dE[\rho_b + \rho_{2D}(E, \mathbf{x})]$$
$$= e(V_f - V_{\overline{\Gamma}})\rho_b + n_{2D}(E_f, \mathbf{x}), \qquad (1)$$

where the surface LDOS is split into the bulk background and surface-state LDOS, ρ_b and $\rho_{2D}(E, \mathbf{x})$, respectively. ρ_b is assumed to be constant, which is a good approximation for a noble metal in the narrow energy interval of interest. $\Sigma(\mathbf{x})$ is directly related to the total electron density $n_{2D}(E_f, \mathbf{x})$ of surface-state electrons with energy $E_{\overline{\Gamma}} < E < eV_f$, i.e., the total density of the electron gas with a "fictitious Fermi level" E_f [see Fig. 2(b)] [12]. The total density of surface-state electrons $n_{2D}(E_f, \mathbf{x})$ can be inferred directly from the measured $\Sigma(\mathbf{x})$ [Eq. (1)]:

$$n_{2D}(E_f, \mathbf{x}) = n_0\left[\frac{\Sigma(\mathbf{x})}{\overline{\Sigma}}\left(1 + \frac{\rho_b}{L_0}\right) - \frac{\rho_b}{L_0}\right], \qquad (2)$$

where $n_0 = L_0(E_f - E_{\overline{\Gamma}})$ is the total density of the free electron gas in the absence of any external potential, $L_0 = m^*/\pi\hbar^2$ is the DOS of the free 2D electron gas, and $\overline{\Sigma}$ is the spatial average of $\Sigma(\mathbf{x})$.

Figure 3(a) shows the total density $n_{2D}(-320$ meV, $\mathbf{x})$ on the reconstructed Au(111) surface. It was obtained from $\Sigma(\mathbf{x})$ using Eq. (2) and the ratio ρ_b/L_0 determined by tunneling spectra taken on clean surface spots right before and after the acquirement of the density map [Fig. 2(c)]. Only those tips were used for potential mapping where the spectra taken on clean terraces proved to be reasonably flat above the surface-state onset, ensuring that the assumption of a constant tip DOS is justified. The total density in Fig. 3(a) shows minima in the fcc regions and maxima on the fcc side of the ridges [see also solid line in Fig. 3(c)]. The total density $n_{2D}(-320$ meV, $\mathbf{x})$ of Fig. 3(a) can be very well understood in terms of the LDOS displayed in Fig. 1(b). Integrating the LDOS of Fig. 1(b) over energies in the corresponding interval $[-520$ meV, -320 meV] actually leads to a density very similar to the one displayed in Fig. 3(c). It is clear from Fig. 1(b) that the maxima in $n_{2D}(-320$ meV, $x)$ lying close to the ridges of the reconstruction are due to the broad LDOS peaks centered at -380 meV.

Starting with the total density of surface-state electrons (with E in $[E_{\overline{\Gamma}}, E_f]$) we now determine the potential using linear response theory. Any potential $U^{\text{tot}}(\mathbf{x})$ acting on an otherwise free electron gas of density n_0 induces rearrangements in the electron density, i.e., the density in the presence of $U^{\text{tot}}(\mathbf{x})$ reads $n(\mathbf{x}) = n_0 + n^{\text{ind}}(\mathbf{x})$ [13]. In linear response theory the Fourier transforms of n^{ind} and U^{tot} are related by the susceptibility $\chi(\mathbf{q})$ [2,14], $n^{\text{ind}}(\mathbf{q}) = \chi(\mathbf{q})U^{\text{tot}}(\mathbf{q})$. For a 2D electron gas, and in linear order perturbation theory, the susceptibility (or so-called Lindhard function) is given by [15]

$$\chi_L(\mathbf{q}) = \begin{cases} -L_0 & \text{for } q \leq 2k_F, \\ -L_0(1 - \sqrt{1 - \frac{4k_F^2}{q^2}}) & \text{for } q > 2k_F, \end{cases} \qquad (3)$$
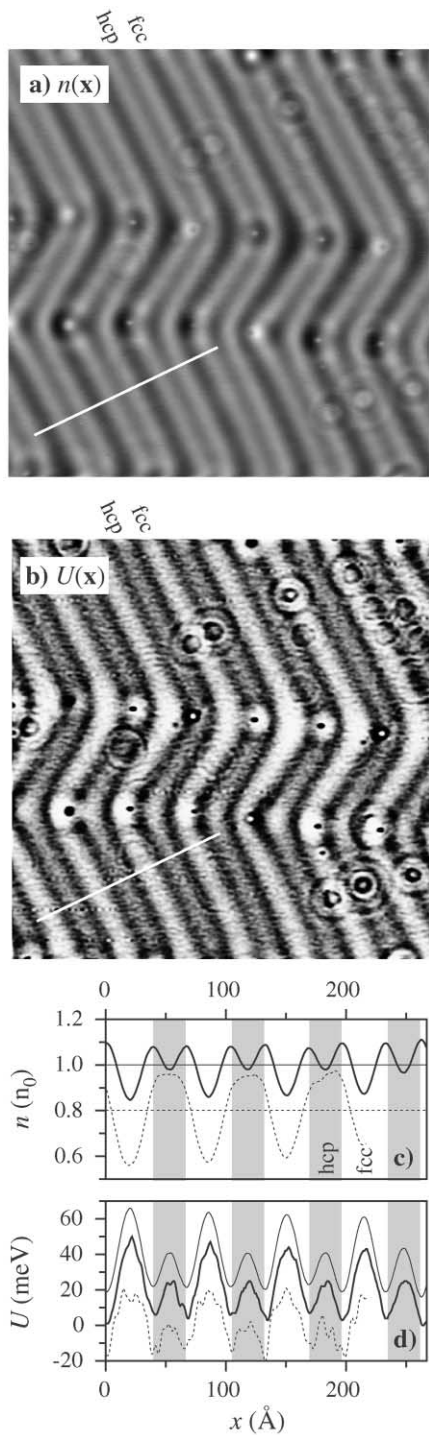
FIG. 3. (a) The 512 Å × 512 Å density map $n_{2D}(-320\,\text{meV}, \mathbf{x})$ acquired simultaneously with the constant-current topograph in Fig. 1(a) ($I = 0.87$ nA, $\nu = 2.43$ kHz). (b) External potential map $U(\mathbf{x})$ obtained by applying the Lindhard procedure to the density of (a) ($k_f = 0.12\,\text{Å}^{-1}$). Dark levels correspond to more attractive potential regions. Solid lines in (c) and (d) show $n_{2D}(-320\,\text{meV}, x)$ and $U(x)$, averaged over some line scans parallel to the white lines in (a) and (b). The thin line in (d) shows the potential derived with the Thomas-Fermi approximation. The dashed lines show $n_{2D}(-450\,\text{meV}, x)$ (offset by $-0.2n_0$ for clarity) and the corresponding $U(x)$.

where $q = |\mathbf{q}|$. The 2D Lindhard function is nonanalytic at $q = 2k_F$ leading to Friedel oscillations [16].

Since the redistribution of electronic charge $-en^{\text{ind}}(\mathbf{x})$ itself contributes to the total potential, the latter is generally different from the external potential acting on the electrons, i.e., in linear response theory $U(\mathbf{q}) = \epsilon(\mathbf{q})U^{\text{tot}}(\mathbf{q})$. In 2D, $\epsilon(\mathbf{q})$ is given by [15]

$$\epsilon(\mathbf{q}) = 1 - \frac{1}{2}\frac{e^2}{\epsilon_b \epsilon_0 q}\chi(\mathbf{q}), \tag{5}$$

where ϵ_b is the dielectric constant of the medium surrounding the electron plane. Since the medium surrounding the 2D surface-state electron gas on noble metals, i.e., the 3D bulk electrons, is highly polarizable, we can set $\epsilon_b \to \infty$ and thus in our case $U(\mathbf{q}) = U^{\text{tot}}(\mathbf{q})$. Altogether, in good approximation, we can relate the external potential to the total density of the Au(111) surface state by

$$n_{2D}(E_f, \mathbf{q}) = \chi_L(\mathbf{q})U(\mathbf{q}). \tag{6}$$

In our case k_F entering the Lindhard function [Eq. (3)] has to be replaced by $k_f = \sqrt{2m^*(E_f - E_{\overline{\Gamma}})/\hbar^2}$.

We wrote a computer program to map the potential. This program performs the fast Fourier transform of the density image $n_{2D}(E_f, \mathbf{x})$, divides this Fourier transform by the Lindhard susceptibility $\chi_L(\mathbf{q})$, and then does an inverse Fourier transformation to yield the potential map $U(\mathbf{x})$. The program was tested by applying the procedure to the total particle density in the presence of weak square potentials, calculated using simple quantum mechanics. The potentials determined with our program for such test electron densities agree very well with the input potentials, minor discrepancies being due to the fact that our procedure relies on *linear* response theory.

Figure 3(b) shows the potential map of the Au(111) surface derived from the total electron density of Fig. 3(a) using the Lindhard approach. The potential modulation due to the herringbone reconstruction is clearly visible. Furthermore, there are features in the potential maps associated with surface and subsurface defects appearing as white and black spots in Fig. 1(a). It is not clear whether these features do represent the real potential, since the different chemical nature of the defects may induce changes in the bulk LDOS, and then the assumption of a constant ρ_b is no more justified. Therefore, we concentrate on the potential modulations induced by the reconstruction. In agreement with Chen *et al.* [5] we find that surface-state electrons are less strongly bound in fcc than in hcp regions. In addition, we find that the regions close to the reconstruction ridges are more attractive than fcc and hcp regions; see the profile in Fig. 3(d).

We now discuss the robustness of our method to the choice of E_f and to tip changes. Clearly, the total electron density $n_{2D}(E_f, \mathbf{x})$ depends on the choice of E_f, i.e., the bias modulation used during the measurement. But of course, if our potential mapping is correct, the resulting external potential should be independent of E_f. This is
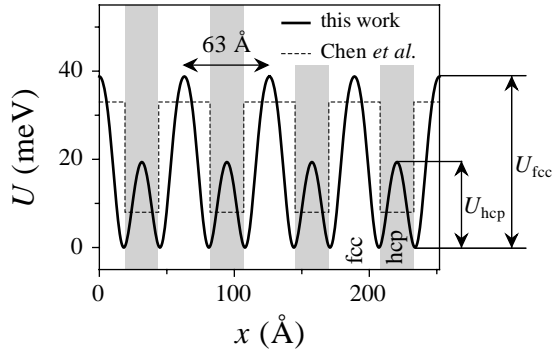
FIG. 4. Electron potential perpendicular to the Au(111) reconstruction lines. The fourth order Fourier series fit to the potential of Fig. 3(d) is compared to the (25 ± 5) meV deep extended Kronig-Penney potential of Ref. [5].

indeed what we observe in all our measurements: densities for E_f in the range of -450 meV to -320 meV yield essentially the same surface potential. This is illustrated for the example of $E_f = -450$ meV by the dashed lines in Figs. 3(c) and 3(d). $n_{2D}(-450 \text{ meV}, x)$ is less structured than $n_{2D}(-320 \text{ meV}, x)$ due to the fact that $k_f(-450 \text{ meV})$ is by about a factor of 2 smaller than $k_f(-320 \text{ meV})$, and therefore $n_{2D}(-450 \text{ meV}, x)$, which can exhibit modulations on length scales not shorter than $2\pi/k_f(-450 \text{ meV})$, is smoother than $n_{2D}(-320 \text{ meV}, x)$. Although the electron density profiles taken at the two fictitious Fermi levels differ substantially, the resulting potentials are identical, except for noise. In the about 20 independent potential measurements we performed, the relative sensitivity of the tip to surface and bulk states, ρ_b/L_0, ranged from 0.7 to 3. Nevertheless, the resulting potential maps proved to be independent of ρ_b/L_0. We also emphasize that an uncertainty in the dispersion relation, i.e., an uncertainty in k_f, does not affect the deduced potentials crucially: varying k_f by $\pm 10\%$ leads to essentially identical potential maps. The thin solid line in Fig. 3(d) shows the potential derived using the Thomas-Fermi approximation [2], $U(x) = -n_{2D}(x)/L_0$. Since the fictitious Fermi wavelength $2\pi/k_f(-320 \text{ meV})$ is with 54 Å comparable to the typical length over which the potential changes, Thomas-Fermi theory works well in this case.

Figure 4 shows the corrugation of the external potential we find for the Au(111)-($\sqrt{3} \times 22$) surface. It has its minima, where surface atoms occupy bridge sites. In hcp regions electrons are less strongly bound by $U_{hcp} = 15 \pm 5$ meV, and in fcc regions even less by $U_{fcc} = 37 \pm 5$ meV. The difference in binding energy between fcc and hcp regions is in excellent agreement with the value found by Chen et al. [5]. However, the real potential shape, in particular, the fact that the bridge sites bind electrons most strongly, could not be revealed by Chen et al. since they interpreted their STS data in the framework of a Kronig-Penney model. In addition to the potential shape across the ($22 \times \sqrt{3}$) unit cell our $U(\mathbf{x})$ map

in Fig. 3(b) also reveals potential changes at the elbows of the mesoscopic reconstruction pattern. There is a further enhancement of $U(\mathbf{x})$ in the fcc regions at the rounded elbows, i.e., the upper row of elbows in Figs. 1(a) and 3(b). Furthermore, for the pointed elbows (lower row), we observe two additional shallow potential minima on the ridge sides of every hcp region. Altogether, our data suggest that electrons are most strongly bound to the surface areas with the highest hydrostatic pressure [17].

In conclusion, we presented a new method to image electron potential landscapes at surfaces. It was applied to the s-p derived surface state on Au(111). Excellent agreement between hcp-fcc-binding energy differences in the measured potential maps and previously published results obtained using traditional scanning tunneling spectroscopy establishes our method as a useful tool to probe electron potentials on atomic length scales.

*Current address: Cavendish Laboratory, Madingley Road, Cambridge CB3 OHE, U.K.

[1] P. Hohenberg and W. Kohn, Phys. Rev. **136**, B864 (1964).
[2] N.W. Ashcroft and N. D. Mermin, *Solid State Physics* (Saunders College, Philadelphia, 1976).
[3] J.V. Barth et al., Phys. Rev. B **42**, 9307 (1990).
[4] P. O. Gartland and B. J. Slagsvold, Phys. Rev. B **12**, 4047 (1975); S. D. Kevan, Phys. Rev. Lett. **50**, 526 (1983); R. Paniago et al., Surf. Sci. **336**, 113 (1995); M. F. Crommie, C. P. Lutz, and D. M. Eigler, Nature (London) **363**, 524 (1993); Y. Hasegawa and P. Avouris, Phys. Rev. Lett. **71**, 1071 (1993).
[5] W. Chen et al., Phys. Rev. Lett. **80**, 1469 (1998).
[6] F. Reinert et al., Phys. Rev. B **63**, 115415 (2001).
[7] D. Fujita et al., Phys. Rev. Lett. **78**, 3904 (1997).
[8] O. Jeandupeux et al., Phys. Rev. B **59**, 15 926 (1999).
[9] To avoid convolution between the electronic structure of interest and the one contributing to the tunnel current used to adjust the tip height, the tip height is stabilized at large positive bias ($V = 1$ V, $I = 2.1$ nA).
[10] G. Hörmandinger, Phys. Rev. B **49**, 13 897 (1994); J. Li, W. D. Schneider, and R. Berndt, ibid. **56**, 7656 (1997).
[11] A. Selloni et al., Phys. Rev. B **31**, 2602 (1985); N. D. Lang, ibid. **34**, 5947 (1986).
[12] Note that $\int_{E_{\bar{\Gamma}}}^{E_f} dE \rho_{2D}(E, \mathbf{x})$ can be interpreted in terms of the electron density $n_{2D}(E_f, \mathbf{x})$ only because e-e interaction in the surface-state electron gas is screened by bulk electrons. If many-body effects were relevant in the 2D gas, the presence of electrons in occupied states with energies in the interval $[E_{\bar{\Gamma}}, E_F]$ would alter the electronic states with $E < E_f$, and thus $\int_{E_{\bar{\Gamma}}}^{E_f} dE \rho_{2D}(E, \mathbf{x})$ could not directly be related to $n_{2D}(E_f, \mathbf{x})$, except for $E_f = E_F$.
[13] We consider only static potentials here.
[14] J. Lindhard, K. Dan. Vidensk. Selsk. Mat. Fys. Medd. **28**, 1 (1954).
[15] F. Stern, Phys. Rev. Lett. **18**, 546 (1967).
[16] J. Friedel, Nuovo Cimento **7**, 287 (1958).
[17] H. Bulou and C. Goyhenex, Phys. Rev. B **65**, 045407 (2002).